

Constraining the Fifth Force Using the Earth as a Spin and Mass Source from the Chinese Space Station

Zheng-Ting Lai,¹ Jun-Xu Lu,^{1,*} Li-Sheng Geng,^{1,2,3,4,†} Kai Wei,^{5,6,7} and Wei Ji^{8,9}

¹*School of Physics, Beihang University, Beijing 102206, China*

²*Peng Huanwu Collaborative Center for Research and Education, Beihang University, Beijing 100191, China*

³*Beijing Key Laboratory of Advanced Nuclear Materials and Physics, Beihang University, Beijing 102206, China*

⁴*Southern Center for Nuclear-Science Theory (SCNT), Institute of Modern Physics, Chinese Academy of Sciences, Huizhou 516000, China*

⁵*School of Instrumentation Science and Opto-electronics Engineering, Beihang University, Beijing 100191, China*

⁶*Hangzhou Innovation Institute, Beihang University, Hangzhou 310051, China*

⁷*Hefei National Laboratory, Hefei 230088, China*

⁸*Johannes Gutenberg University, Mainz 55128, Germany*

⁹*Helmholtz-Institut, GSI Helmholtzzentrum für Schwerionenforschung, Mainz 55128, Germany*

We explore the potential of conducting an experiment on the Chinese Space Station (CSS) to constrain beyond-the-standard-model (BSM) long-range spin- and velocity-dependent interactions, which are mediated by the exchange of an ultralight ($m_{z'} < 10^{-10}$ eV) or massless intermediate vector boson. We demonstrate that the proposed experiment on the CSS offers several advantages compared to ground-based experiments. The high speed can enhance the sensitivity to velocity-dependent interactions. The periodicity allows efficient extraction of signals from background noises, thereby strengthening the experiment's accuracy. Combining these advantages, one can improve the existing bounds on such interactions by up to five orders of magnitude. With advancements in sensor technology, we anticipate a further enhancement of four orders of magnitude, resulting in a total potential improvement of up to nine orders of magnitude.

Introduction.— The Standard Model of Particle Physics (SM) has proven to be the most successful theory for describing the fundamental building blocks of nature and their interactions. Various approaches across multiple fields of physics have extensively tested it. However, new physics beyond the SM is eagerly sought to explain unresolved phenomena such as dark matter [1], dark energy [2], strong CP violation [3], the matter-antimatter asymmetry [4], and the hierarchy problem [5]. Among the numerous attempts to extend the Standard Model, the idea of an additional fundamental interaction—beyond the well-known strong, weak, electromagnetic, and gravitational forces—has emerged as one of the most promising solutions. This hypothetical interaction is often called the fifth force [6, 7].

Hypothetical fifth forces can generally be classified into two categories: those that depend on spins [8–10] and those that do not [11]. The former, also known as exotic spin-dependent interactions, could be interpreted as new types of long-range forces mediated between fermions via novel light or massless particles including spin-0 axion-like particles (ALPs) [3, 12, 13], spin-1 bosons [9], and dark photons [14, 15], all of which are also leading candidates for dark matter or dark energy.

Moody and Wilczek first proposed the formalism for the exotic spin-dependent interactions associated with the axion [8]. Later, it was shown that any interaction mediated by scalar and vector bosons can be expressed via 16 individual terms with their spin, mass, distance, and relative velocity [9]. These potentials were revisited recently [10], where they were categorized by the types of physical couplings instead of the spin-momentum structure [9]. Meanwhile, various experiments have been proposed or performed to search for them, such as

torsion balance or pendulum experiments [16–20], resonance string experiments [21], spectroscopy [22, 23], comagnetometers [24–29], trapped ions [30], nitrogen-vacancy center in diamond [31, 32], neutron or polarized ³He atoms [33] or other macroscopic experiments [34–36]. These experiments typically use a large collection of particles as a polarized spin source or an unpolarized mass source, and spin sensors, i.e., sensitive systems for measuring the resulting shifts in spin energy levels.

Depending on the size of the spin source, these experiments can be roughly divided into two categories: those using laboratory sources and those using the Earth [28, 34–38], the Moon or the Sun [39–41] as an enormous source. B.R. Heckel proposed to utilize the unpolarized matter in the Earth or the Sun to search for exotic velocity-dependent potentials between polarized electrons and unpolarized matter in the Sun and Moon [39]. Later, L. Hunter proposed utilizing the Earth as an enormous polarized geoelectron source to investigate exotic spin- and velocity-dependent interactions [35, 36]. Despite the additional loss due to the distance from the polarized electrons and nucleons to the sensor, the enormous geoelectron and nucleon source significantly improves the sensitivity of detecting exotic spin- and velocity-dependent interactions [34–36]. Relevant studies include experiments carried out by researchers from the National Institute of Standards and Technology [42], the University of Washington [37], Amherst College [34–36, 43], Tsinghua University [44], and California State University [38].

Compared to laboratory detection, the main drawbacks of using the Earth as a spin or mass source are the inability to modulate the source and the location of the experiment artificially, as well as the limited relative velocity originating

from the Earth's rotation. Motivated by these limitations, we propose placing a spin sensor in the Chinese Space Station (CSS), which offers a relative speed of about 7800 meters per second, approximately 30 times that of the ground-based experiments [35, 36, 39]. The CSS also covers the Earth's surface between 42° north and south latitude, allowing experiments to be conducted in diverse locations, a key advantage as emphasized in Refs. [34, 45]. Temporally, with the space station circling the Earth and its self-rotation, one anticipates unique periodic signals due to the geomagnetic field. Spatially, measurements can be performed at any position, enabling the exploration of the most stringent constraints under the same sensitivity. Overall, this experiment has unique advantages for force ranges exceeding one kilometer compared to former ground-based experiments.

Framework.— We focus on velocity-dependent interactions in the present work. To better demonstrate the proposed experiment's advantages, we use the same framework employed by L. Hunter [35]. Following Ref. [46], the six exotic velocity-dependent spin-spin interactions are:

$$V_{6,7} = -\frac{\hbar}{8\pi c^2} \left(\frac{g_V^1 g_A^2}{2M_1} + \frac{g_A^1 g_V^2}{2M_2} \right) \times [(\hat{\sigma}_1 \cdot \mathbf{v})(\hat{\sigma}_2 \cdot \hat{\mathbf{r}}) \pm (\hat{\sigma}_1 \cdot \hat{\mathbf{r}})(\hat{\sigma}_2 \cdot \mathbf{v})] \times \left(1 + \frac{r}{\lambda} \right) \frac{e^{-r/\lambda}}{r^2}, \quad (1)$$

$$V_8 = \frac{g_A^1 g_A^2}{4\pi c^2} [(\hat{\sigma}_1 \cdot \mathbf{v})(\hat{\sigma}_2 \cdot \mathbf{v})] \frac{e^{-r/\lambda}}{r}, \quad (2)$$

$$V_{14} = \frac{g_A^1 g_A^2}{4\pi c} [(\hat{\sigma}_1 \times \hat{\sigma}_2) \cdot \mathbf{v}] \frac{e^{-r/\lambda}}{r}, \quad (3)$$

$$V_{15} = -\frac{g_V^1 g_V^2 \hbar^2}{8\pi c^3 M_1 M_2} \times [(\hat{\sigma}_1 \cdot (\mathbf{v} \times \hat{\mathbf{r}}))(\hat{\sigma}_2 \cdot \hat{\mathbf{r}}) + (\hat{\sigma}_1 \cdot \hat{\mathbf{r}})(\hat{\sigma}_2 \cdot (\mathbf{v} \times \hat{\mathbf{r}}))] \times \left(3 + \frac{3r}{\lambda} + \frac{r^2}{\lambda^2} \right) \frac{e^{-r/\lambda}}{r^3}, \quad (4)$$

$$V_{16} = -\frac{\hbar}{8\pi c^3} \left(\frac{g_V^1 g_A^2}{2M_1} + \frac{g_A^1 g_V^2}{2M_2} \right) \times [(\hat{\sigma}_1 \cdot (\mathbf{v} \times \hat{\mathbf{r}}))(\hat{\sigma}_2 \cdot \mathbf{v}) + (\hat{\sigma}_1 \cdot \mathbf{v})(\hat{\sigma}_2 \cdot (\mathbf{v} \times \hat{\mathbf{r}}))] \times \left(1 + \frac{r}{\lambda} \right) \frac{e^{-r/\lambda}}{r^2}, \quad (5)$$

where $g_{V/A}$ denotes the vector (V) or axial (A) coupling constant of fermion 1 or 2 with spins $\hat{\sigma}_{1/2}$ and masses $M_{1,2}$. The distance and relative speed between the two fermions are denoted by r and \mathbf{v} , $\hat{\mathbf{r}}$ is the unit vector of relative coordinate, $\lambda = \hbar/m'c$ is the reduced Compton wavelength of the boson of interest of mass m' , representing the scale of the forces, \hbar is the reduced Planck constant, and c is the speed of light in a vacuum.

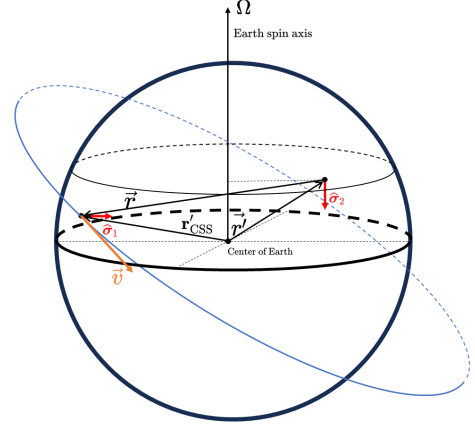


FIG. 1: Schematic layout of the proposed experiment. $\hat{\sigma}_1$ represents the spin-sensitive direction of the apparatus on the CSS, and $\hat{\sigma}_2$ represents the direction opposite to the geomagnetic field. \mathbf{r}'_{CSS} and \mathbf{r}' represent the radial position vector of the CSS and the goelectron, respectively.

Although V_{4+5} could not provide the most stringent bounds as those lowest-order terms, it can probe different spin/velocity structures and confirm which types of couplings the exchanged boson has. Meanwhile, V_{12+13} has the form of a Yukawa potential multiplied by the factor $\boldsymbol{\sigma} \cdot \mathbf{v}$, which may provide the only access to some couplings that might vanish in velocity-independent cases [7]. Similarly, the proposed experiment can also shed light on these two interactions due to the much larger relative velocity, which read [7, 36, 47]:

$$V_{4+5}|_{VV} = \frac{g_V^e g_V^N}{16\pi m_e} \boldsymbol{\sigma}_e \cdot (\mathbf{v} \times \hat{\mathbf{r}}) \left(\frac{1}{r^2} + \frac{1}{\lambda r} \right) e^{-\frac{r}{\lambda}}, \quad (6)$$

$$V_{4+5}|_{AA} = \frac{g_A^e g_A^N}{16\pi} \frac{m_e}{m_N^2} \boldsymbol{\sigma}_e \cdot (\mathbf{v} \times \hat{\mathbf{r}}) \left(\frac{1}{r^2} + \frac{1}{\lambda r} \right) e^{-\frac{r}{\lambda}}, \quad (7)$$

$$V_{12+13} = g_A^1 g_V^2 \frac{\hbar}{4\pi} \boldsymbol{\sigma}_1 \cdot \mathbf{v} \frac{e^{-r/\lambda}}{r}. \quad (8)$$

We first establish a model for the Earth to describe the exotic velocity-dependent interactions between the Earth as the source and the spin sensor on the CSS. The model involves its goelectron density [34, 48–50] and nucleon density [36, 48, 51, 52], which are both denoted by $\rho(r')$, the internal temperatures $T(r')$ [53], where r' represents the distance between the source particle and the center of the Earth, as well as the distribution of the geomagnetic field, B , both inside and outside the Earth. For further details, we refer to the Supplemental Material.

If the exotic interactions are not detected, V_{total} would be less than the energy bound established by the spin coupling energy measured by the spin sensor in the sensitive direction, as in various experiments. This, in turn, sets the upper bounds for the unknown coupling constants of the fifth force.

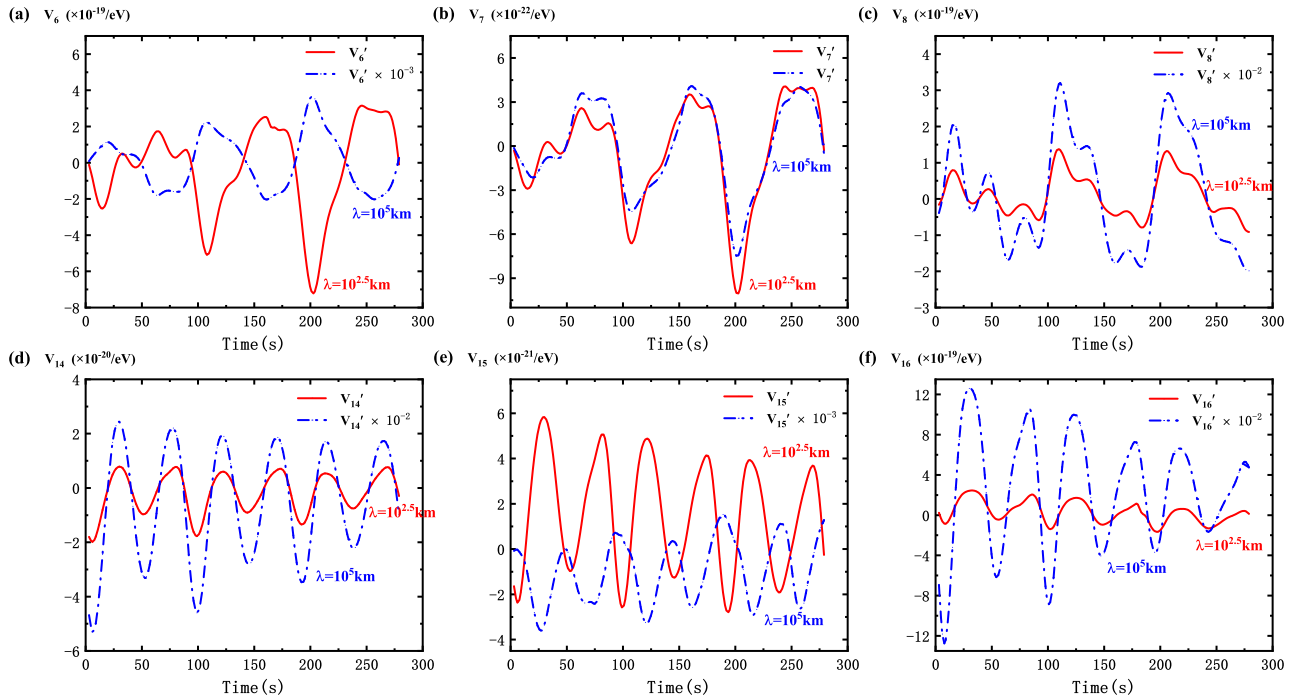


FIG. 2: Periodicity of expected signals. The starting point of the Time axis is arbitrarily chosen to be July 1st 2024.

Results and discussions.— Due to the Yukawa-type $e^{-r/\lambda}$ factor, more geoelectrons and nucleons in the mantle contribute as λ increases. For $\lambda = 10^{2.5}$ km, this approximates the CSS orbital altitude, while for $\lambda = 10^5$ km, it is roughly twice the Earth’s radius, beyond which the potentials saturate. Therefore, in the following, we take $\lambda = 10^{2.5}$ km or $\lambda = 10^5$ km as typical examples to show the results. For λ well below the CSS’s altitude, the improvements due to the high speed will be suppressed since the minimal r is the orbit altitude rather than approximately zero, as in ground-based experiments.

In Ref. [34], using the measurements from two local Lorentz in-variance experiments [39, 54], bounds on the coupling constants of different velocity-dependent spin-spin interactions between two electrons for various ranges of λ were obtained. In the present work, to demonstrate the periodicity of the signal expected in the proposed experiment, we first take these bounds for electron-electron (e - e) interactions between velocity-dependent spin-spin potentials as inputs to extract V'_{total} to be measured on the CSS. The expected results corresponding to $\lambda = 10^{2.5}$ km and $\lambda = 10^5$ km are shown in Fig. 2.

All these potentials show clear periodicity as the CSS orbits the Earth. Such periodicity will be beneficial for extracting signals from background noises, thereby improving the experiment’s accuracy. Additionally, the line shapes of various interactions differ significantly, indicating the possibility of distinguishing the contributions from these exotic interactions in the proposed experiment. This provides unique opportuni-

ties to determine the magnitude of the couplings and identify the types of interactions observed.

Once the CSS’s trajectory covers the entire area, we can create a contour plot identifying the most sensitive position for each interaction. This can be determined as shown in the Supplemental Material, resulting in the lowest bounds for the coupling constants. In Fig. 3, we present the expected lowest bounds for all six exotic velocity-dependent spin-spin interactions’ couplings for e - e interactions as functions of the effective range λ , assuming the same sensitivity as the spin sensors used in the LLI experiment in Seattle. In that experiment, the upper limits on the interactions were measured to be $\beta_N < 5.9 \times 10^{-21}$ eV oriented north and $\beta_E < 8 \times 10^{-22}$ eV oriented east.

Similar to the bounds obtained in the ground-based experiment [35], the bounds on the e - e couplings with spin-oriented north (N) are usually not as stringent as those with spin-oriented east (E). The coupling constants for most interactions are expected to be more constrained by at least three orders of magnitude. In those less sensitive regions, an improvement of at least one order of magnitude can still be expected.

The bounds on the couplings of V_6 (Fig. 3(a)) are approximately 2.4 orders of magnitude more restrictive than those in Refs. [34, 35] for $\lambda = 10^{2.5}$ km, and at least 1.3 orders of magnitude more constrained in the flatter regions. For V_7 (Fig. 3(b)), the bounds on the couplings are lowered by approximately 1.6 orders of magnitude across the entire range. In addition, the proposed experiment can measure V_6 for λ less than 10^2 km, which is inaccessible to previous experi-

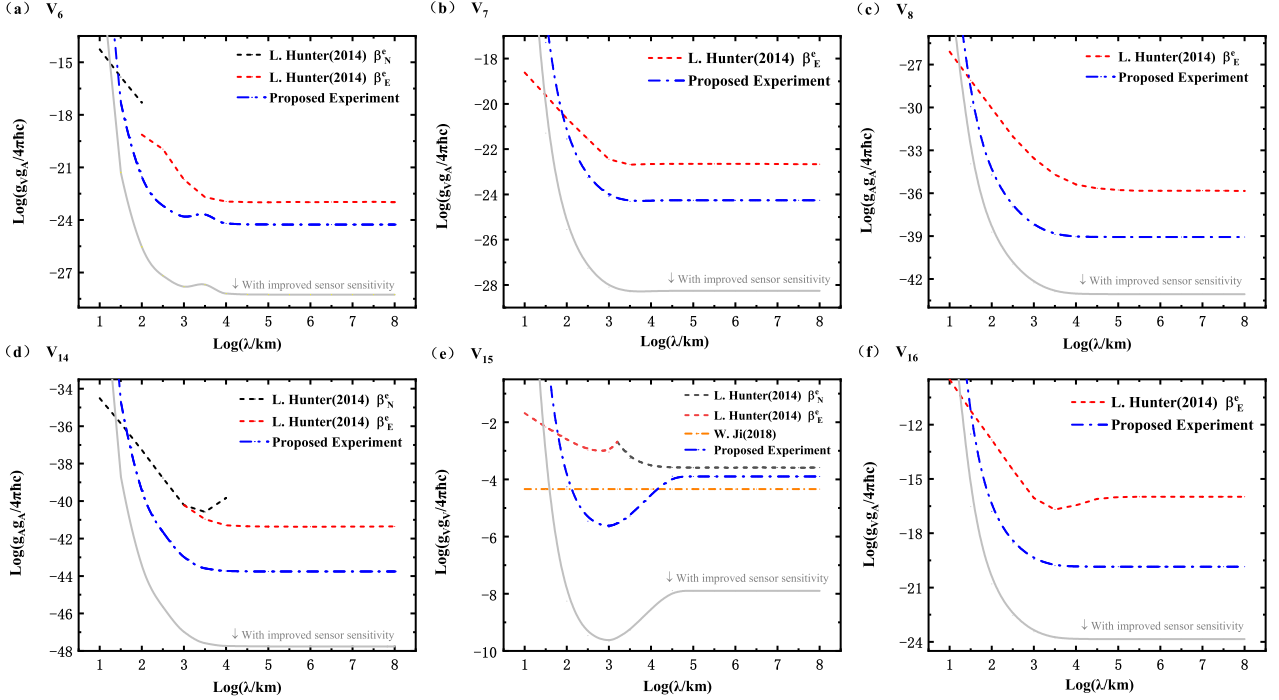


FIG. 3: Expected bounds on long-range spin-spin velocity-dependent couplings for electron-electron (e - e) interactions. The blue curves represent the expected constraints with the sensory precision of Ref. [34, 35]. (a) Vector-axial (V-A) couplings [Eq. 1 with the + sign] for V_6 . (b) (V-A) couplings [Eq. 1 with the - sign] for V_7 . (c) (A-A) couplings [Eq. 2] for V_8 . (d) (A-A) couplings [Eq. 3] for V_{14} . (e) (V-V) couplings [Eq. 4] for V_{15} . (f) (V-A) couplings [Eq. 5] for V_{16} .

ments [35]. Moreover, since V_{6+7} would be more meaningful than V_6 or V_7 individually for experiments [7], based on Fig. 3(a) and Fig. 3(b), we can further constrain V_{6+7} , which is shown in the Supplemental Material.

The constraints on V_8 (Fig. 3(c)) can improve by up to five orders of magnitude for $\lambda = 10^{2.5}$ km and by at least 3.2 orders of magnitude in the flatter regions. The upper limits for V_{16} (Fig. 3(f)) are further lowered by up to four orders of magnitude for $\lambda = 10^{2.5}$ km and are at least three orders of magnitude more constrained in the flatter regions.

The upper limits for V_{14} (Fig. 3(d)) decrease by up to three orders of magnitude for $\lambda = 10^{2.5}$ km and by at least 2.5 orders of magnitude for $\lambda = 10^5$ km. For V_{15} (Fig. 3(e)), the behavior is quite different. The couplings are approximately three orders of magnitude more restrictive for $\lambda = 10^{3.5}$ km compared to Refs. [34, 35], while as λ increases, the improvement becomes less pronounced, indicating a more sensitive λ dependence. In Ref. [35], V_{15} is found to be less reliable than other potentials, especially at short ranges, because it is more susceptible to local inhomogeneities. On the other hand, the proposed experiment can overcome this limitation and provide a more accurate constraint.

Meanwhile, for the long-range spin-velocity dependent interactions for electron-nucleon (e - N) interactions, we find that the improvement is mainly in the region where λ is longer than the height of the CSS. As depicted in Fig. 4, the improve-

ment is around 1.5 orders of magnitude in the flatter areas. At the same time, similar to the spin-spin velocity-dependent interactions, the progress is most significant when $\lambda = 10^{2.5}$ km. For $V_{4+5}|_{VV}$ and $V_{4+5}|_{AA}$ (Fig. 4(a) and Fig. 4(b)), the improvement can be approximately 2.5 orders of magnitude. In contrast, it is two orders of magnitude for the odd-parity spin-velocity term V_{12+13} (Fig. 4(b)). We note that the constraints on $V_{4+5}|_{VV}$ can set new limits on the vector coupling constant g_V of the z' particle. See the Supplemental Material for more details.

Furthermore, impressive improvements have been made in sensor sensitivity, such as the K-Rb- ^{21}Ne co-magnetometer proposed for future experiments, which can offer improvement of one to three orders of magnitude [55]. Compared to the previous experiments with energy resolutions around $10^{-21} \sim 10^{-22}$ eV/Hz $^{1/2}$, the proposed experiments equipped with the newly developed spin sensor are expected to achieve 10^{-23} eV/Hz $^{1/2}$. Moreover, after 100 hours of accumulations, an additional three orders of magnitude would be further enhanced. We thus anticipate an overall extra improvement by four orders of magnitude [29, 56] once the novel spin sensor is utilized, as depicted in Fig. 3 and Fig. 4.

Summary.— In the present work, we proposed a novel approach to constrain further the coupling constants of long-range velocity-dependent interactions, i.e., the fifth force. Taking the Earth as an enormous source, we propose placing

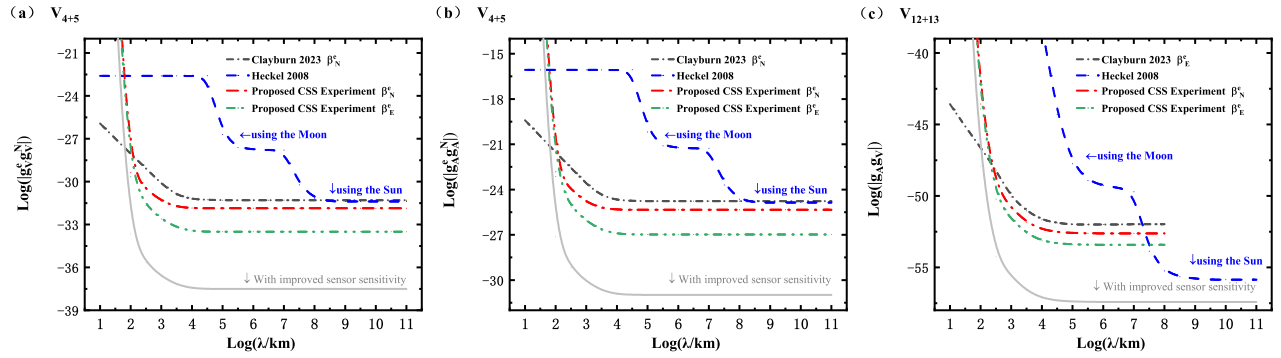


FIG. 4: Expected bounds on long-range spin-velocity-dependent couplings for electron-nucleon (e - N) interactions. The red and green curves in the figure represent the expected constraints with the sensory precision of Ref. [36]. (a) (V - V) couplings [Eq. 6] for $V_{4+5}|_{VV}$. (b) (A - A) couplings [Eq. 7] for $V_{4+5}|_{AA}$. (c) (A - V) couplings [Eq. 8] for V_{12+13} .

the spin sensor on the Chinese Space station to overcome the limitations of ground-based experiments, such as fixed positions and slow speed. Based on the periodic movement of the CSS, we simulate the strength of the interactions. Additionally, by utilizing the speed of the CSS in the near-earth orbit, which is much higher than that in any ground-based experiments, the bounds on most of the six velocity-dependent spin-spin interactions are expected to be at least three orders of magnitude more restrictive than earlier measurements. In contrast, the bounds on the two spin-velocity terms are expected to be more restrictive at least 1.5 orders of magnitude. Specifically, for V_8 , V_{14} , and V_{16} , the improvements could be up to four or five orders of magnitude.

Previous works [34, 45] have underscored the importance of the location of such experiments. In our study, the flexibility of the CSS allows it to cover different regions over time and identify optimal locations for detecting the fifth force with its varying velocities. We believe such an experiment will be highly efficient in pinpointing the best areas to achieve the strongest signals, thereby significantly enhancing the current limits.

Meanwhile, the line shapes from various interactions differ significantly from one another. This indicates the possibility of distinguishing the contributions from these interactions in the proposed experiment and further identifying the dominant one. Such periodicity will also be beneficial for extracting signals from background noises, thereby improving the experiment's accuracy.

Acknowledgement.— This work is partly supported by the National Key R&D Program of China under Grant No. 2023YFA1606700 and the National Science Foundation of China under Grant No. 12435007.

* Corresponding author: ljxwohool@buaa.edu.cn

† Corresponding author: lisheng.geng@buaa.edu.cn

[1] G. Bertone, D. Hooper, and J. Silk,

Phys. Rept. **405**, 279 (2005), [arXiv:hep-ph/0404175](https://arxiv.org/abs/hep-ph/0404175).

- [2] J. Frieman, M. Turner, and D. Huterer, *Ann. Rev. Astron. Astrophys.* **46**, 385 (2008), [arXiv:0803.0982](https://arxiv.org/abs/0803.0982) [astro-ph].
- [3] R. D. Peccei and H. R. Quinn, *Phys. Rev. Lett.* **38**, 1440 (1977).
- [4] M. Dine and A. Kusenko, *Rev. Mod. Phys.* **76**, 1 (2003), [arXiv:hep-ph/0303065](https://arxiv.org/abs/hep-ph/0303065).
- [5] P. W. Graham, D. E. Kaplan, and S. Rajendran, *Phys. Rev. Lett.* **115**, 221801 (2015), [arXiv:1504.07551](https://arxiv.org/abs/1504.07551) [hep-ph].
- [6] M. S. Safronova, D. Budker, D. DeMille, D. F. J. Kimball, A. Derevianko, and C. W. Clark, *Rev. Mod. Phys.* **90**, 025008 (2018), [arXiv:1710.01833](https://arxiv.org/abs/1710.01833) [physics.atom-ph].
- [7] L. Cong *et al.*, (2024), [arXiv:2408.15691](https://arxiv.org/abs/2408.15691) [hep-ph].
- [8] J. E. Moody and F. Wilczek, *Phys. Rev. D* **30**, 130 (1984).
- [9] B. A. Dobrescu and I. Mocioiu, *JHEP* **11**, 005 (2006), [arXiv:hep-ph/0605342](https://arxiv.org/abs/hep-ph/0605342).
- [10] P. Fadeev, Y. V. Stadnik, F. Ficek, M. G. Kozlov, V. V. Flambaum, and D. Budker, *Phys. Rev. A* **99**, 022113 (2019), [arXiv:1810.10364](https://arxiv.org/abs/1810.10364) [hep-ph].
- [11] E. G. Adelberger, B. R. Heckel, and A. E. Nelson, *Ann. Rev. Nucl. Part. Sci.* **53**, 77 (2003), [arXiv:hep-ph/0307284](https://arxiv.org/abs/hep-ph/0307284).
- [12] F. Wilczek, *Phys. Rev. Lett.* **40**, 279 (1978).
- [13] S. Weinberg, *Phys. Rev. Lett.* **40**, 223 (1978).
- [14] J. Jaeckel and A. Ringwald, *Ann. Rev. Nucl. Part. Sci.* **60**, 405 (2010), [arXiv:1002.0329](https://arxiv.org/abs/1002.0329) [hep-ph].
- [15] H. An, M. Pospelov, J. Pradler, and A. Ritz, *Phys. Lett. B* **747**, 331 (2015), [arXiv:1412.8378](https://arxiv.org/abs/1412.8378) [hep-ph].
- [16] G. D. Hammond, C. C. Speake, C. Trenkel, and A. Pulido Paton, *Phys. Rev. Lett.* **98**, 081101 (2007).
- [17] B. R. Heckel, W. A. Terrano, and E. G. Adelberger, *Phys. Rev. Lett.* **111**, 151802 (2013).
- [18] W. A. Terrano, E. G. Adelberger, J. G. Lee, and B. R. Heckel, *Phys. Rev. Lett.* **115**, 201801 (2015), [arXiv:1508.02463](https://arxiv.org/abs/1508.02463) [hep-ex].
- [19] J. Ding *et al.*, *Phys. Rev. Lett.* **124**, 161801 (2020).
- [20] T. C. P. Chui and W.-T. Ni, *Phys. Rev. Lett.* **71**, 3247 (1993).
- [21] J. C. Long, H. W. Chan, A. B. Churnside, E. A. Gulbis, M. C. M. Varney, and J. C. Price, *Nature* **421**, 922 (2003), [arXiv:hep-ph/0210004](https://arxiv.org/abs/hep-ph/0210004).

- [22] F. Ficek, D. F. J. Kimball, M. Kozlov, N. Leefer, S. Pustelny, and D. Budker, *Phys. Rev. A* **95**, 032505 (2017), [arXiv:1608.05779 \[physics.atom-ph\]](#).
- [23] F. Ficek, P. Fadeev, V. V. Flambaum, D. F. Jackson Kimball, M. G. Kozlov, Y. V. Stadnik, and D. Budker, *Phys. Rev. Lett.* **120**, 183002 (2018), [arXiv:1801.00491 \[physics.atom-ph\]](#).
- [24] G. Vasilakis, J. M. Brown, T. W. Kornack, and M. V. Romalis, *Phys. Rev. Lett.* **103**, 261801 (2009), [arXiv:0809.4700 \[physics.atom-ph\]](#).
- [25] N. Crescini, G. Carugno, P. Falferi, A. Ortolan, G. Russo, and C. C. Speake, *Phys. Rev. D* **105**, 022007 (2022), [arXiv:2011.07100 \[hep-ex\]](#).
- [26] D. Wu, H. Liang, M. Jiao, Y.-F. Cai, C.-K. Duan, Y. Wang, X. Rong, and J. Du, *Phys. Rev. Lett.* **131**, 071801 (2023), [arXiv:2308.02254 \[hep-ex\]](#).
- [27] H. Liang, M. Jiao, Y. Huang, P. Yu, X. Ye, Y. Wang, Y. Xie, Y.-F. Cai, X. Rong, and J. Du, *Nat. Sci. Rev.* **10**, nwac262 (2023).
- [28] S. Zhang, Z. Ba, D. Ning, N. Zhai, Z. Lu, and D. Sheng, *Phys. Rev. Lett.* **130**, 201401 (2023), [arXiv:2303.10352 \[gr-qc\]](#).
- [29] K. Wei, W. Ji, C. Fu, A. Wickenbrock, J. Fang, V. V. Flambaum, and D. Budker, *Nature Commun.* **13**, 7387 (2022), [arXiv:2203.07050 \[physics.atom-ph\]](#).
- [30] S. Kotler, R. Ozeri, and D. F. J. Kimball, *Phys. Rev. Lett.* **115**, 081801 (2015), [arXiv:1501.07891 \[physics.atom-ph\]](#).
- [31] X. Rong *et al.*, *Nature Commun.* **9**, 739 (2018), [arXiv:1706.03482 \[quant-ph\]](#).
- [32] X. Rong, M. Jiao, J. Geng, B. Zhang, T. Xie, F. Shi, C.-K. Duan, Y.-F. Cai, and J. Du, *Phys. Rev. Lett.* **121**, 080402 (2018), [arXiv:1804.07026 \[hep-ex\]](#).
- [33] H. Yan, G. A. Sun, S. M. Peng, Y. Zhang, C. B. Fu, H. Guo, and B. Q. Liu, *Phys. Rev. Lett.* **115**, 182001 (2015), [arXiv:1412.8155 \[nucl-ex\]](#).
- [34] L. Hunter, J. Gordon, S. Peck, D. Ang, and J. F. Lin, *Science* **339**, 928 (2013).
- [35] L. R. Hunter and D. Ang, *Phys. Rev. Lett.* **112**, 091803 (2014), [arXiv:1306.1118 \[hep-ph\]](#).
- [36] N. B. Clayburn and L. R. Hunter, *Phys. Rev. D* **108**, L051701 (2023), [arXiv:2306.05327 \[hep-ph\]](#).
- [37] B. J. Venema, P. K. Majumder, S. K. Lamoreaux, B. R. Heckel, and E. N. Fortson, *Phys. Rev. Lett.* **68**, 135 (1992).
- [38] D. F. Jackson Kimball, J. Dudley, Y. Li, D. Patel, and J. Valdez, *Phys. Rev. D* **96**, 075004 (2017), [Erratum: *Phys. Rev. D* **107**, 019903 (2023)], [arXiv:1707.00745 \[physics.atom-ph\]](#).
- [39] B. R. Heckel, E. G. Adelberger, C. E. Cramer, T. S. Cook, S. Schlamminger, and U. Schmidt, *Phys. Rev. D* **78**, 092006 (2008), [arXiv:0808.2673 \[hep-ex\]](#).
- [40] L. Y. Wu, K. Y. Zhang, M. Peng, J. Gong, and H. Yan, *Phys. Rev. Lett.* **131**, 091002 (2023), [arXiv:2302.09096 \[hep-ph\]](#).
- [41] N. Leefer, A. Gerhardus, D. Budker, V. V. Flambaum, and Y. V. Stadnik, *Phys. Rev. Lett.* **117**, 271601 (2016), [arXiv:1607.04956 \[physics.atom-ph\]](#).
- [42] D. J. Wineland, J. J. Bollinger, D. J. Heinzen, W. M. Itano, and M. G. Raizen, *Phys. Rev. Lett.* **67**, 1735 (1991).
- [43] A. N. Youdin, D. Krause, K. Jagannathan, L. R. Hunter, and S. K. Lamoreaux, *Phys. Rev. Lett.* **77**, 2170 (1996).
- [44] W.-T. Ni, S.-S. Pan, H.-C. Yeh, L.-S. Hou, and J.-L. Wan, *Phys. Rev. Lett.* **82**, 2439 (1999).
- [45] Y. Tian and D. Zhao, *PHYSICS OF THE EARTH AND PLANETARY INTERIORS* **200**, 72 (2012).
- [46] B. A. Dobrescu, *Phys. Rev. Lett.* **94**, 151802 (2005), [arXiv:hep-ph/0411004](#).
- [47] P. H. Chu, N. Ristoff, J. Smits, N. Jackson, Y. J. Kim, I. Savukov, and V. M. Acosta, *Phys. Rev. Res.* **4**, 023162 (2022), [arXiv:2112.14882 \[quant-ph\]](#).
- [48] A. M. Dziewonski and D. L. Anderson, *Physics of the Earth and Planetary Interiors* **25**, 297 (1981).
- [49] T. Irifune, T. Shinmei, C. A. McCammon, N. Miyajima, D. C. Rubie, and D. J. Frost, *Science* **327**, 193 (2010).
- [50] R. Jeanloz, E. Knittle, R. K. O'Nions, R. Clayton, and B. Parsons, *Philosophical Transactions of the Royal Society of London. Series A, Mathematical and Physical Sciences* **371**, 20190116 (2019).
- [51] J. W. Morgan and E. Anders, *Proceedings of the National Academy of Sciences* **77**, 6973 (1980).
- [52] H. S. Wang, C. H. Lineweaver, and T. R. Ireland, *Icarus* **299**, 460 (2018).
- [53] B. Buffett and W. Davis, *Geophysical Research Letters* **45**, 1845 (2018).
- [54] S. K. Peck, D. K. Kim, D. Stein, D. Orbaker, A. Foss, M. T. Hummon, and L. R. Hunter, *Phys. Rev. A* **86**, 012109 (2012), [arXiv:1205.5022 \[physics.atom-ph\]](#).
- [55] L. Cong, W. Quan, K. Wei, X. Huang, X. Ma, W. Ji, and J. Liu, *JAIS* **2024**, 505 (2024), [arXiv:2312.09491 \[hep-ex\]](#).
- [56] Z. Xu *et al.*, *Commun. Phys.* **7**, 226 (2024), [arXiv:2309.16600 \[hep-ph\]](#).
- [57] F. D. Stacey, *Physics of the Earth and Planetary Interiors* **15**, 341 (1977).
- [58] A. Chulliat *et al.*, *The US/UK World Magnetic Model for 2020-2025: Technical Report*, Tech. Rep. (US/UK, 2020).
- [59] B. A. Buffett, E. J. Garnero, and R. Jeanloz, *Science* **290**, 1338 (2000).
- [60] S. K. Peck, D. K. Kim, D. Stein, D. Orbaker, A. Foss, M. T. Hummon, and L. R. Hunter, *Phys. Rev. A* **86**, 012109 (2012).

SUPPLEMENTAL MATERIAL

Model of the Earth and the CSS

The model is based on Ref. [34], which assumes that the Earth's paramagnetism is predominantly due to unpaired d -shell electrons in the iron ions contained within the Earth's mantle and crust minerals. Using this assumption, the density of geoelectrons was calculated. In the model, density and temperature distributions are considered spherically symmetric, and the Earth's core magnetization is assumed to be negligible, as predicted by density functional theory calculations [35]. Additionally, we adopted the temperature model from Ref. [57], along with the updated World Magnetic Model (WMM 2020) [58, 59], which is valid from 2020 to 2025 for the Earth's magnetic field.

The planetary position and velocity of the CSS can be accurately obtained using the Skyfield package with the corresponding TLE code. In this work, we use $\mathbf{v}(r', \theta', \varphi', r'_{\text{CSS}}, \theta'_{\text{CSS}}, \varphi'_{\text{CSS}})$ to represent the relative velocity between the spin sensor on the space station and a specific geoelectron in the Earth's mantle. Here, $r', \theta', \varphi', r'_{\text{CSS}}, \theta'_{\text{CSS}},$ and φ'_{CSS} denote the spherical coordinates of the geoelectron and the space station, respectively, with the center of the Earth as the origin, as shown in Fig. 1. The velocity resulting from the Earth's rotation is given by $\mathbf{v}' = \boldsymbol{\Omega} \times \mathbf{r}'$. By combining this with \mathbf{v}'_{CSS} , we can determine the relative velocity $\mathbf{v} = \mathbf{v}'_{\text{CSS}} - \mathbf{v}'$, which is necessary for our calculations.

When summing up the interactions between each polarized geoelectron inside the Earth and the spin sensor on the CSS, the total potential can be calculated as follows:

$$V_{\text{total}} = \int_0^{2\pi} \int_0^\pi \int_{R_{\text{CM}}}^{R_s} r'^2 \sin \theta' \rho(r') \frac{2\mu_B B}{k_B T(r')} \times V(\mathbf{r}, \mathbf{v}) dr' d\theta' d\varphi', \quad (9)$$

where μ_B is the Bohr magneton, k_B is the Boltzmann constant, and T is the temperature. The integration is over all the volume from the core-mantle boundary (R_{CM}) to the surface (R_s). Note that the relative speed \mathbf{v} is the sum of the Earth's rotation and the speed of the CSS, which is far beyond the velocities achievable in laboratory settings [36].

We modulated the Earth as a nucleon source for the two spin-velocity terms. To calculate the expected potentials between the electron and the nucleon, we can calculate the potentials as follows:

$$V_{\text{total}} = \int_0^{2\pi} \int_0^\pi \int_0^{R_s} r'^2 \sin \theta' \rho(r') \times V(\mathbf{r}, \mathbf{v}) dr' d\theta' d\varphi', \quad (10)$$

The difference from the e - e study is that the $\rho(r')$ here represents the density of Earth's un-polarized nucleon density instead of the polarized electron density. Also, the integration should cover the entire space of the Earth, i.e., from the center of the Earth to the surface (R_s).

Counter Plot

In Fig. 5, we use the TLE code mentioned earlier to generate the contour plot. Due to the vector-based geographic relationships involved in the calculations, the potential measured at a given position may vary depending on the direction the CSS approaches. This means that the potential detected when the CSS travels from south to north may differ from when it travels from north to south. However, as long as the TLE data remains unchanged, the contour plot will stay fixed. Consequently, as the CSS orbits the Earth, the signals it receives will exhibit periodicity with each orbit. Although slight differences may arise between the signals due to the variation in angular velocities, the overall periodicity is sufficient to apply some signal processing techniques to help distinguish signals from background noises, thereby improving the experiment's accuracy.

In previous works [34, 45], it was proposed that conducting experiments in southern Thailand would yield about twice the sensitivity compared to those performed in Amherst due to the stronger and more parallel surface magnetic field in Thailand. This highlights the importance of the experiment's location. In our study, the flexibility of the space station allows it to cover different regions over time, enabling the identification of optimal locations for detecting new interactions with varying velocities. We believe such an experiment will be highly efficient in pinpointing the best areas for achieving the strongest signals, thus significantly improving the sensitivity limits.

Compared to the previous works by L. Hunter et al. [34, 35, 60], we found that the bounds on the electron (e) energy, when its spin is oriented north (N), are generally less restrictive than when oriented east (E). This suggests that the most restrictive bounds are likely to be obtained through measurements in the eastward direction. Another key difference is that, unlike experiments conducted on Earth, the potential of long-range interactions, V' , does not always maintain the same sign in space. As the CSS orbits the Earth, the angles between $\hat{\sigma}_1, \hat{\sigma}_2, \mathbf{r}$, and \mathbf{v} continuously change. As a result, it is natural to observe the potential oscillating between positive and negative values, as illustrated in Fig. 2.

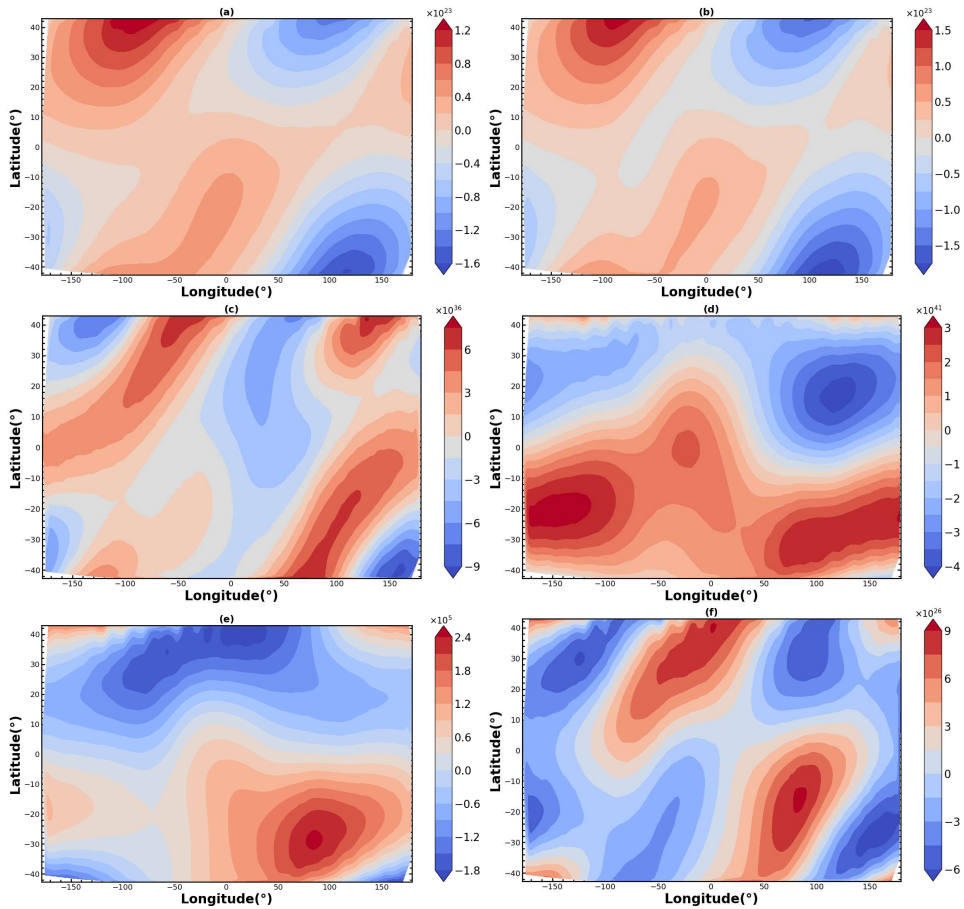


FIG. 5: Contour plots of the potentials expected as the CSS travels from south to north. (a) V_6 . (b) V_7 . (c) V_8 . (d) V_{14} . (e) V_{15} . (f) V_{16} .

Constrain on V_{6+7}

Among all the 16 potentials mentioned in Ref. [9], certain potentials, for instance, $V_{4,5}$ and $V_{6,7}$ are symmetric and (anti)symmetric concerning the exchange of the particle spins. However, in experiments employing one polarized test mass and one spin source, only a linear combination of V_6 and V_7 , i.e., $V_{6\pm 7}$, is accessible [7]. As a matter of fact, we study V_{6+7} in the following, which reads:

$$V_{6+7} = -\frac{\hbar}{4\pi c^2} \left(\frac{g_V^1 g_A^2}{2M_1} + \frac{g_A^1 g_V^2}{2M_2} \right) \times [(\hat{\sigma}_1 \cdot \mathbf{v})(\hat{\sigma}_2 \cdot \hat{\mathbf{r}})] \times \left(1 + \frac{r}{\lambda} \right) \frac{e^{-r/\lambda}}{r^2} \quad (11)$$

Using the same method mentioned above, we can constrain the potential with Eq. 9. The bounds on the Vector-Axial (V-A) couplings of V_{6+7} (Fig. 6) are approximately 1.7 orders of magnitude more restrictive than those in Refs. [34, 35] for $\lambda = 10^{2.5}$ km, and at least 1.4 orders of magnitude more constrained in the flatter regions.

New Limits on the z' Particle

The proposed experiment can set new limits on $|f_{4+5}| \leq 8.2 \times 10^{-32}$ for neutron-nucleon (n - N) interactions and $|f_{4+5}| \leq 1.5 \times 10^{-29}$ for proton-nucleon (p - N) interactions for a force range of $\lambda \geq 10^{5.5}$ km with the sensory precision of Ref. [36, 38, 54]. Similar to Ref. [29], we can set new limits on the vector coupling constant g_V of the z' particle.

To give an expected upper limit on the z' particle, we assume that the sensor has the same neutron and proton mass contribution and fraction factors for neutron and proton polarization in the ^{21}Ne nucleus of Ref. [29], i.e., $\zeta_n^{\text{Ne}} = 0.58$, $\zeta_p^{\text{Ne}} = 0.04$ and the neutron and proton mass contribution in the Earth is $\zeta_n^{\text{Earth}} = 0.514$ and $\zeta_p^{\text{Earth}} = 0.486$ [36].

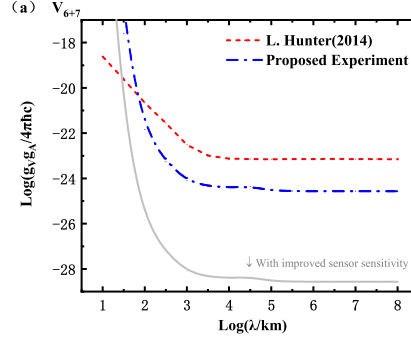


FIG. 6: Expected bounds on long-range spin-spin velocity-dependent couplings for electron-electron (e - e) interactions. The blue curve represents the expected constraints with the sensory precision of Ref. [34, 35].

From $f_{4+5} = \frac{1}{2}g_A g_A - \frac{3}{2}g_V g_V$, assuming that $g_A g_A = 0$, we have

$$|(\zeta_p^{\text{Ne}} g_V^p + \zeta_n^{\text{Ne}} g_V^n) (\zeta_p^{\text{Earth}} g_V^p + \zeta_n^{\text{Earth}} g_V^n)| \leq 5.5 \times 10^{-32}. \quad (12)$$

If we set $g_V^p = 0$ in Eq. 12, we can constrain the $|g_V^n| \leq 4.3 \times 10^{-16}$. Meanwhile, if $g_V^n = 0$, we can constrain the $|g_V^p| \leq 1.7 \times 10^{-15}$.

Assuming that $g_V g_V = 0$, we have

$$|(\zeta_p^{\text{Ne}} g_A^p + \zeta_n^{\text{Ne}} g_A^n) (\zeta_p^{\text{Earth}} g_A^p + \zeta_n^{\text{Earth}} g_A^n)| \leq 1.6 \times 10^{-31}. \quad (13)$$

If we set $g_A^p = 0$ in Eq. 13, we can constrain the $|g_A^n| \leq 7.3 \times 10^{-16}$. Meanwhile, if $g_A^n = 0$, we can constrain the $|g_A^p| \leq 2.9 \times 10^{-15}$.

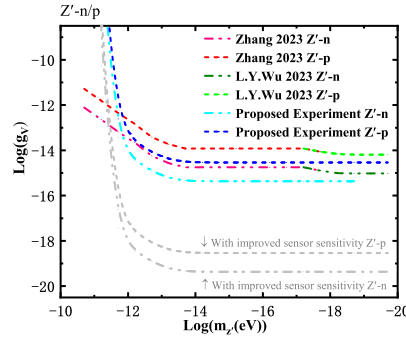


FIG. 7: Expected constraint on the z' particle. The red and blue dash-dotted curves represent the expected constraints with the sensory precision of Ref. [36, 38, 54].

In Fig. 7, we compare the current limits and the expected constraint from the proposed experiment on g_V , which is the vector coupling constant between z' and standard model particles. The bounds on the z' (Fig. 7) are approximately 0.8 orders of magnitude more restrictive than those in Refs. [28] for $m_{z'} = 10^{-12.2045}$ eV ($\lambda = 10^{2.5}$ km), and at least 0.6 orders of magnitude more constrained in the flatter regions.